Article

Deformation Prediction Theory of Thermal Barrier Coatings near Cooling Holes under Thermal Cycling

Jian-Xin Wang, Hong-Tu Sun, Qing-Tao Gong, Feng-Xun Li,* and Zhen-Zhe Li*

Read Online

ACCESS | 📊 Metrics & More | 📖 Article Recommendations

ABSTRACT: Thermal barrier coating (TBC) systems are widely adopted in gas turbine blades to improve the thermal efficiency of gas turbine engines. However, TBC failure will happen due to the thermal stress between the different layers of the TBC systems. The traditional two-layer theoretical model only considers TGO (thermally grown oxide) and a substrate in the inner cooling hole with the surface uncoated, which results in poor prediction of the deformations of the TBC systems. It should be mentioned that the effect of TBC is very important because the thickness of TBC is much larger than the TGO thickness. In this study, a new three-layer theoretical model was derived, which is composed of the cylindrical TGO and TBC mounted in the substrate with a circular hole, and the stress and strain of TGO near the cooling hole under the condition of the thermal cycles were calculated. The high temperature characteristics of TGO and the substrate including the high temperature strength and growth ratio were from the experiments. The results

show that the strain of the developed three-layer model is irrelevant with increasing number of cycles, which indicates that TBC in the cooling hole significantly inhibits the deformation of TGO near the cooling hole. Therefore, aimed at confirming the feasibility of the three-layer theoretical model, the finite element analysis with coating in the cooling hole and on the surface was carried out with a three-layer axisymmetric model, which proves that the 3-layer theoretical model can predict the deformation trend near the cooling hole.
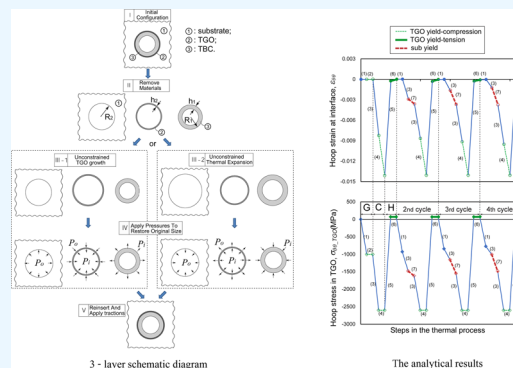
1. INTRODUCTION

The efficiency of the gas turbine engine for the aircraft is significantly related to the level of the operating temperature which is promoted to higher than 1700 °C. The film cooling technology of the turbine blade and the thermal barrier coating systems (TBCs) are the effective heat insulation methods[1−5] to improve the thermal tolerance and antioxidant capacity of the gas turbine engines continuously.

TBCs are composed of TBC, underlying substrates (super-alloy), BC (bond coat), and TGO (thermally grown oxide). Although TGO can protect the underlying super-alloy from hot corrosion, it is also the main cause of the invalidation of TBCs.[6,7]

The failure of TBCs is mainly due to the TGO growth, which is divided into the thickness direction (transverse) and the lateral (in-plane). Because of the difference of the thermal expansion coefficients (CTEs) between TGO and other layers, the stress increases with the increase of TGO thickness.[8,9] The thermal expansion coefficients of TBC and BC are $10 \times 10^{-6}/$°C, which are similar with the substrate ($12 \times 10^{-6}/$°C), but the TGO layer has a very low CTE of $6 \times 10^{-6}/$°C. During the heating or cooling process, TGO will cause a stress of 3∼6GPa.[1,10,11] Furthermore, the thermal cycles will cause the microcracks or TBC separation at the interface of TGO/BC or

TGO/TBC. The other growth of the TGO is in the lateral direction. At the operating temperatures, the new TGO forms along the existing TGO grains boundaries, and pushes the existing TGO grains toward lateral sides, leading to the compressive stress in the TGO layer, i.e., TGO growth stress.[12,13]

For the gas turbine blade, air cooling hole technology is widely used except TBCs, which construct air film to protect the turbine blade from hot corrosion.[14−18] Most studies on the cooling holes focused on the analysis of heat insulation efficiency of the TBC. The failure mechanism of TBC in the turbine blades could be more complicated. During the operation of the turbine engine, not only the thermal fatigue but also the thermal stress caused by the CTE difference of each layer of TBCs, the influence of structure and thermal load must be considered.
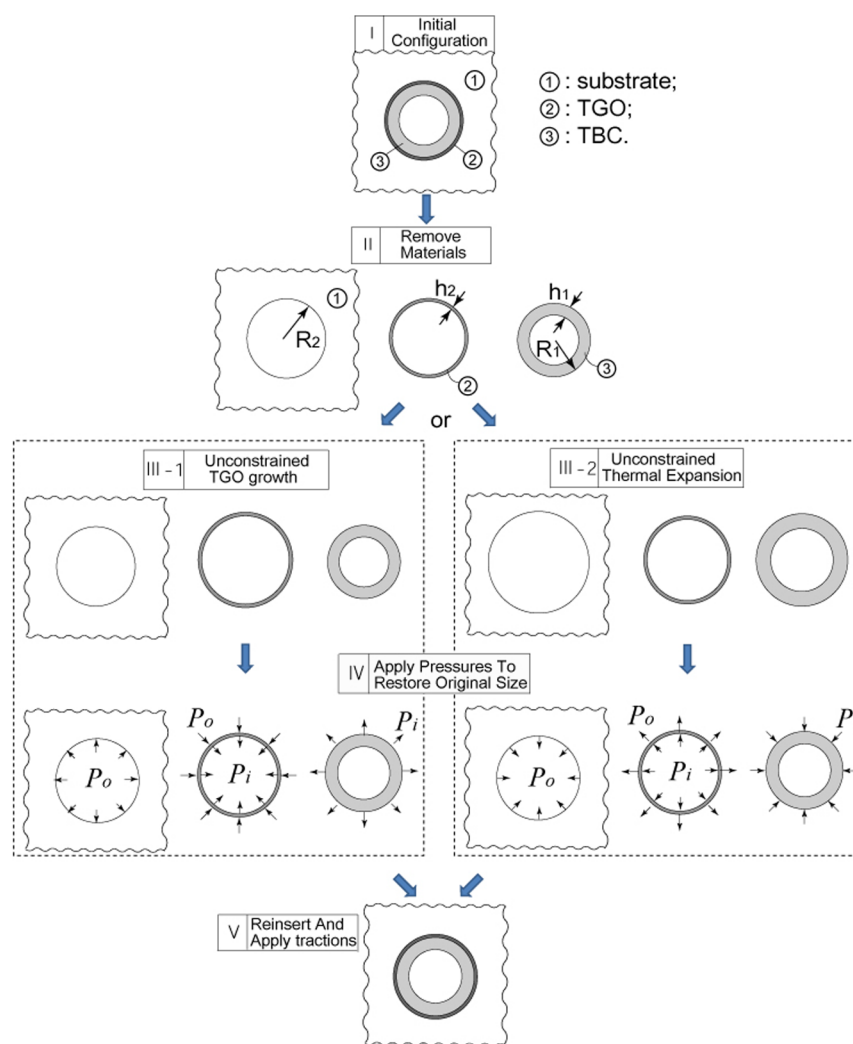
Figure 1. Schematic diagram of the derivation process: (1) substrate; (2) TGO; and (3) TBC.

Li et al.[19] investigated the plastic deformation and micro-crack initiation behavior near the cooling holes by using the in situ tension test at ambient temperatures. The results revealed that the cooling holes have reduced the tensile strength of the Ni-based alloy by about 10%, and the cracks near the cooling holes initiate along the slip lines.

Zhao et al.[20] conducted creep fatigue experiments on tubular specimens with the cooling holes. They found that the fracture of the cooling hole is caused by the stress concentration and high temperature deformation, which will produce initial cracks along the edge of the hole.

According to the fracture research results of TBC by Jiang et al.,[21] two fracture forms were found around the sample with the cooling hole after the thermal cycle, namely, the surface crack and the interface crack of the finish coat. However, during the sample processing, the TBC inside the cooling hole was removed because TBC blocks the cooling hole. If there is TBC inside the cooling hole, the stress concentration near the cooling hole may be more serious.

Rebollo et al.[22] made a groove on the surface of FeCr alloy sample, and the thermal fatigue experiments were performed in the high temperature environment. The results show that TGO near the groove at a constant temperature has not been changed, but the groove after thermal fatigue processing has been significantly changed. Also, it is found that deformation

under the conditions of constant temperature and cyclic oxidation can be significantly restrained when TBC is added. In order to recognize the deformation mechanism of the microcracks clearly, Evans et al.[23,24] performed series of theoretical and finite element simulations. At first, a spherical and theoretical model, which is composed of TGO and BC was constructed, and TGO deformations near the groove under the thermal cycling were analyzed. Also, the theoretical model was verified using the finite element analysis. However, the material properties in their research were assumed data such as the constant yield strengths of TGO and BC for every temperature.

In our previous study,[25−27] a 2-layer theoretical model was derived to study the hole deformation under the thermal cycling loads. However, the results of the 2-layer theoretical model give good agreement on the behavior of the hole with the TGO layer forming on the inner surfaces as well as the lateral outer surface of the hole. Although the results are very accurate, the experimental and theoretical models focused on the two layers of TGO and the substrate, which has some limitations in predicting the deformation of the real TBC system.

In this paper, the mechanical behavior of the cooling holes under thermal cycling was analyzed by using a new three-layer model for TBCs. By establishing a three-layer theoretical

analysis model, the stress and deformation near the cooling hole under thermal cycling were tracked and analyzed. In order to clarify the deformation mechanism of the cooling hole and the feasibility of theoretical analysis, the finite element analysis was carried out by using the material parameters measured experimentally.

2. ANALYTICAL SOLUTION

A 3-layer theoretical model for the hole deformation distribution was derived using a method similar to that reported by Li et al.,[25] i.e., first, the TGO growth and thermal deformation were allowed to occur unconstrained, and then the required traction pressure was applied to ensure the continuity of displacement and traction.

Figure 1 shows the schematic diagram of the derivation process. In the figure, p_i and p_o are the internal and external pressure of the TGO, respectively.

TBC and TGO were thin cylindrical shells with initial thickness h_1 and h_2, with the radii of R_1 and R_2 (0.5 mm) mounted on infinite metal substrates with a hole. The substrate and the TGO layer were assumed to be elastic and perfectly plastic, and their yield strengths varied with temperature. TBC was assumed to be perfectly elastic.

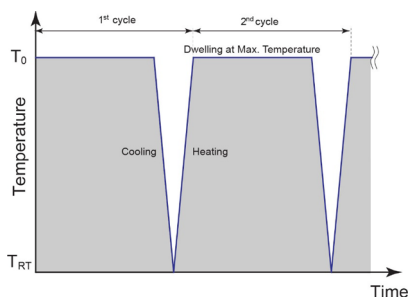The mathematical details are shown below. One cycle consists of TGO growth, cooling, and reheating (Figure 2).

Figure 2. Temperature history for typical thermal cycles.

TGO growth occurs at the maximum temperature T_o and the system is driven by the TGO growth strain ε_g. The TGO growth will not occur during the steps of cooling and reheating; instead, the system is driven by the CTE mismatch between the substrate, TGO, and TBC.

In order to constitute the complete thermal history, the following four combinations are required: (a) the TBC, TGO, and the substrate deformed elastically; (b) TGO remains elastic while the substrate is plastic; and (c) vice versa; (d) TGO and the substrate deformed plastically.

First, when TBC, TGO, and the substrate have elastic responses, the strain and stress in TBC, TGO, and the substrate are as follows based on the internal and external pressure solutions of the hollow cylinder in the plane stress condition:[28]

$$\sigma_{rr\_TBC} = -p_i \tag{1}$$

$$\sigma_{\theta\theta\_TBC} = -p_i \frac{2R_1^2 - 2R_1h_1 + h_1^2}{2R_1h_1 - h_1^2} \tag{2}$$

$$\sigma_{rr\_TGO} = -p_o \tag{3}$$

$$\sigma_{\theta\theta\_TGO} = \frac{R_2}{h_2}(p_i - p_o) \tag{4}$$

$$\sigma_{rr\_sub} = -p_o \tag{5}$$

$$\sigma_{\theta\theta\_sub} = p_o \tag{6}$$

$$\varepsilon_{\theta\theta\_TBC} = \frac{M}{2G_{TBC}} \tag{7}$$

$$\varepsilon_{\theta\theta\_TGO} = \frac{R_2^2}{E_{TGO}h_2}(p_i - p_o) \tag{8}$$

$$\varepsilon_{\theta\theta\_sub} = \frac{p_o}{2G_{sub}} \tag{9}$$

Here,

$$M = \frac{\frac{1-v_{TBC}}{1+v_{TBC}} + \left(\frac{R_1 - h_1}{R_1}\right)^2}{1 - \left(\frac{R_1 - h_1}{R_1}\right)^2} \tag{10}$$

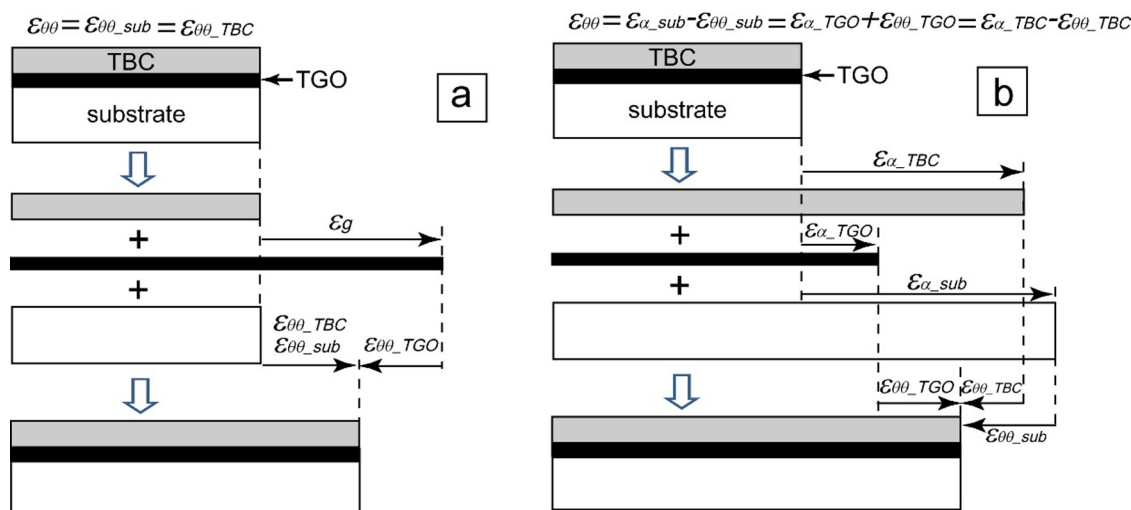**Figure 3.** Determination of the actual strain (a) during TGO growth and (b) during cooling or reheating.

where, σ and ε are the stress and strain, respectively. The subscripts rr and $\theta\theta$ denote the radial and hoop direction, respectively.

Because of the difference of deformations in the processes of TGO growth and reheating (or cooling), the calculations of p_i and p_o are as follows:

Dwelling at the maximum temperature,

$$p_i = \varepsilon_g \left[-M\frac{1}{G_{TBC}}\left(\frac{1}{2} + \frac{G_{sub}R_2}{E_{TGO}h_2}\right) - \frac{R_2}{E_{TGO}h_2} \right]^{-1} \quad (11)$$

$$p_o = p_i M \frac{G_{sub}}{G_{TBC}} \quad (12)$$

During heating or cooling,

$$p_i = \left[-\Delta T(\alpha_{TBC} - \alpha_{TGO}) + \frac{2G_{sub}\Delta T(\alpha_{sub} - \alpha_{TBC})R_2}{E_{TGO}h_2} \right]$$
$$\left[-\frac{M}{G_{TBC}} - \frac{R_2}{E_{TGO}h_2}\left(1 + \frac{MG_{sub}}{G_{TBC}}\right) \right]^{-1} \quad (13)$$

$$p_o = -p_i M \frac{G_{sub}}{G_{TBC}} - 2G_{sub}\Delta T(\alpha_{sub} - \alpha_{TBC}) \quad (14)$$

where G, E, v, and α are the shear modulus, Young's modulus, Poisson's ratio, and CTE, respectively. The subscripts sub, TBC, and TGO denote the substrate, TBC, and TGO layers, respectively. Here, depending on the segment of the thermal history (cooling/reheating or the TGO growth), the actual hoop strains occurring in the processes of TGO growth and cooling/reheating are different from each other. Figure 3 illustrates the schematics. Namely, the actual hoop strain during the TGO growth is the same as that given by eqs 7 and 9, whereas the strain during cooling/reheating is $\varepsilon_{\alpha\_sub} - \varepsilon_{\theta\theta\_sub}$, $\varepsilon_{\alpha\_TGO} + \varepsilon_{\theta\theta\_TGO}$, or $\varepsilon_{\alpha\_TBC} - \varepsilon_{\theta\theta\_TBC}$. Here, ε_α is the strain caused by the temperature change.

The Mises yield criterion was applied to the yield conditions of the TGO layer and the substrate.

First, it is assumed that when the TGO layer yields, the external and internal pressures remain constant, so the stress or strain in TBC, TGO, or the substrate remains constant. Second, when an area near the hole on the substrate is in the yield state, plastic deformation occurs in this area, i.e., that in $R \leq r \leq R_P$ (where R_P is the plastic radius). According to Kaliszky,[29] R_P versus the external pressure and R_P versus $\varepsilon_{\theta\theta\_sub}$ are related by eqs 15 and 16:

$$p_o = \frac{1}{\sqrt{3}}\left(1 + 2\ln\frac{R_P}{R_2}\right)\sigma_Y^{sub} \quad (15)$$

$$\varepsilon_{\theta\theta\_sub} = \frac{\varepsilon_Y^{sub}}{2\sqrt{3}}\left[(5 - 4v_{sub})\left(\frac{R_P}{R_2}\right)^2 - 3(1 - 2v_{sub}) \right.$$
$$\left. \left(1 + 2\ln\frac{R_P}{R_2}\right) \right] \quad (16)$$

where ε_Y^{sub} and σ_Y^{sub} are the yield strain and stress of the substrate, respectively. In addition, $\varepsilon_Y^{sub} = \sigma_Y^{sub}/E_{sub}$. Because the TGO layer is still elastic, the strain and stress in the TGO layer can be obtained by substituting eq 15 into eqs 3~5 and 8.

According to Figure 3b, the relationship between the hoop strain and terminal expansion in TBC, TGO, and the substrate is as follows.

$$\varepsilon_{\theta\theta\_TGO} + \varepsilon_{\theta\theta\_TBC} = \Delta T(\alpha_{TBC} - \alpha_{TGO}) \quad (17)$$

$$\varepsilon_{\theta\theta\_sub} + \varepsilon_{\theta\theta\_TGO} = \Delta T(\alpha_{sub} - \alpha_{TGO}) \quad (18)$$

Since the internal pressure can be calculated by substituting eqs 7, 8, 15, 16 into 17 and 18,

$$p_i = \left[-\Delta T(\alpha_{sub} - \alpha_{TBC}) - \frac{\varepsilon_Y^{sub}}{2\sqrt{3}}\left[(5 - 4v_{sub})\left(\frac{R_P}{R_2}\right)^2 \right. \right.$$
$$\left. \left. - 3(1 - 2v_{sub})\left(1 + 2\ln\frac{R_P}{R_2}\right) \right] \right]/M$$

When the pressure reaches the yield condition of TGO, pressure is assumed to remain constant.

3. MATERIAL PROPERTIES

The properties of elastic materials are the same as those reported in the study of Li et al.,[25,30] and they are listed in Table 1. Regardless of the temperature, these properties are

Table 1. Material Properties of the TBC, TGO Layer, and Substrate

material	Young's modulus, E	Poisson's ratio, v	thermal expansion coefficient, α
TBC	100 GPa	0.25	$12 \times 10^{-6}/°C$
TGO	390 GPa	0.25	$6 \times 10^{-6}/°C$
substrate	140 GPa	0.25	$12 \times 10^{-6}/°C$

assumed to be constant. As shown in Figure 4, the yield strengths of TGO and the substrate are the functions of temperature. The TBC layer is assumed to be perfectly elastic.

Because TGO is a brittle material, the compressive strength and tensile strength are different and depend on the temperature. Namely, under tension (Figure 4a), the TGO yield strength is $\sigma_Y^{sub} = 260$ MPa up to 900 °C, and $\sigma_Y^{sub} = 70$ MPa at 1200 °C. Under compression (Figure 4b), the TGO yield strength is $\sigma_Y^{sub} = -2600$ MPa up to 900 °C, and $\sigma_Y^{sub} = 1000$ MPa at 1200 °C, which was measured in house.[31] In the middle temperature range, the yield stress decreases linearly with temperature. For the substrate (Figure 4c), the yield strength up to 300 °C is $\sigma_Y^{sub} = 200$ MPa, and the yield strength is $\sigma_Y^{sub} = 7.6$ MPa at the temperature above 900 °C, which was also measured in house.[31] The yield stress decreases linearly with the temperature in the middle temperature range.

The TGO growth strain, including the lateral and thickness growth strain, was measured from the author's previous study.[32] Figure 5 shows the variation of h_2 and the lateral growth strain.

4. ANALYTICAL RESULTS

Figure 6a shows the strain variation at the interface, $\varepsilon_{\theta\theta}$, and the lower line in Figure 6b shows the stress variation in the TGO layer, $\sigma_{\theta\theta\_TGO}$, according to the initial four thermal cycles.

In the first cycle, there are six stages.

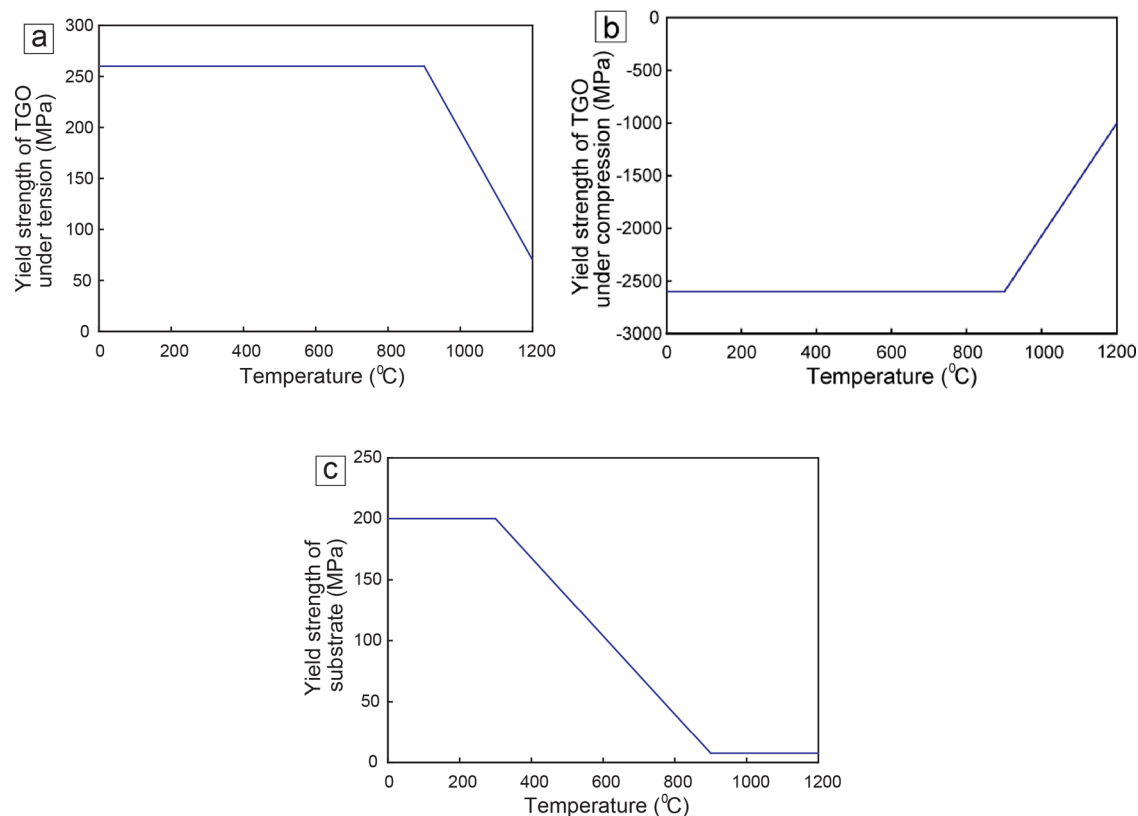(1) Initially, TBC and the substrate respond elastically to the TGO growth in the lateral direction, and eqs 11 and 12

Figure 4. Variation of yield strengths with temperature of (a) TGO under tension, (b) TGO under compression, and (c) substrate.
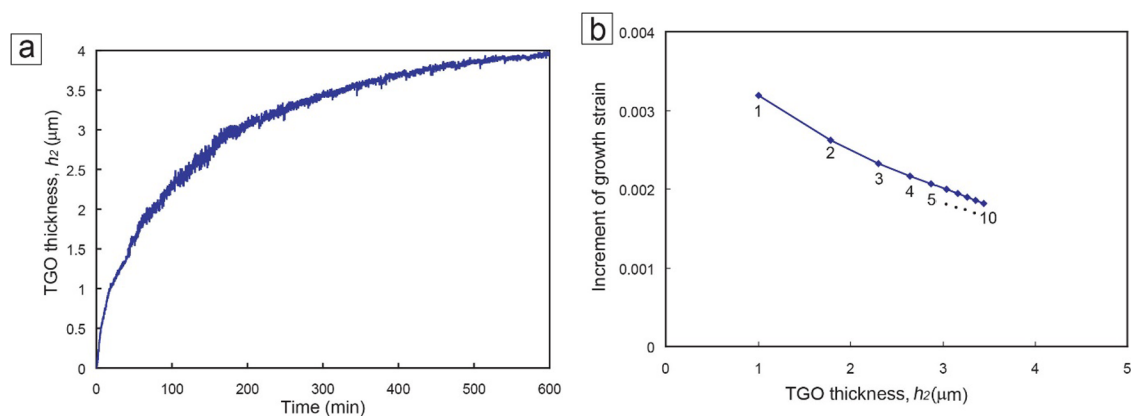

Figure 5. (a) Variation of TGO thickness with oxidation time at 1200 °C, (b) variation of the lateral growth strain of TGO with cycles and the TGO thickness.

can be applied until the substrate or the TGO layer begins to yield.

(2) Under continuing to let the TGO growth yield first, p_i and p_o remain constant; consequently, the strains or stresses in TBC, TGO, and the substrate remained constant according to eqs 1−9.

During cooling and reheating, the following four stages occur.

(3) With the decrease of temperature, the yield strength of TGO increases according to Figure 4b, and the TGO layer responds elastically.

(4) After the temperature drops to 900 °C, TGO becomes constant, and the yield strength of the substrate increases until the temperature drops to 300 °C.

Therefore, the TGO layer yields at a certain temperature around 400 °C, and p_i and p_o remain constant. The stresses in TBC, TGO, and the substrate remain constant according to eqs 1−9, whereas the strain is given by the sum of strains caused by pure thermal shrinkage.

(5) During heating up, the thermal expansion mismatch is reduced and the substrate as well as TGO respond elastically (reversed yield in the substrate was neglected). Eqs 11 and 12 were applied.

(6) When heating up to over a certain temperature, tensile stress occurs in the TGO layer due to the compressive plastic deformation of TGO in the previous cooling step. Because the tensile strength of TGO is much smaller than the compressive strength, TGO is prone to tensile
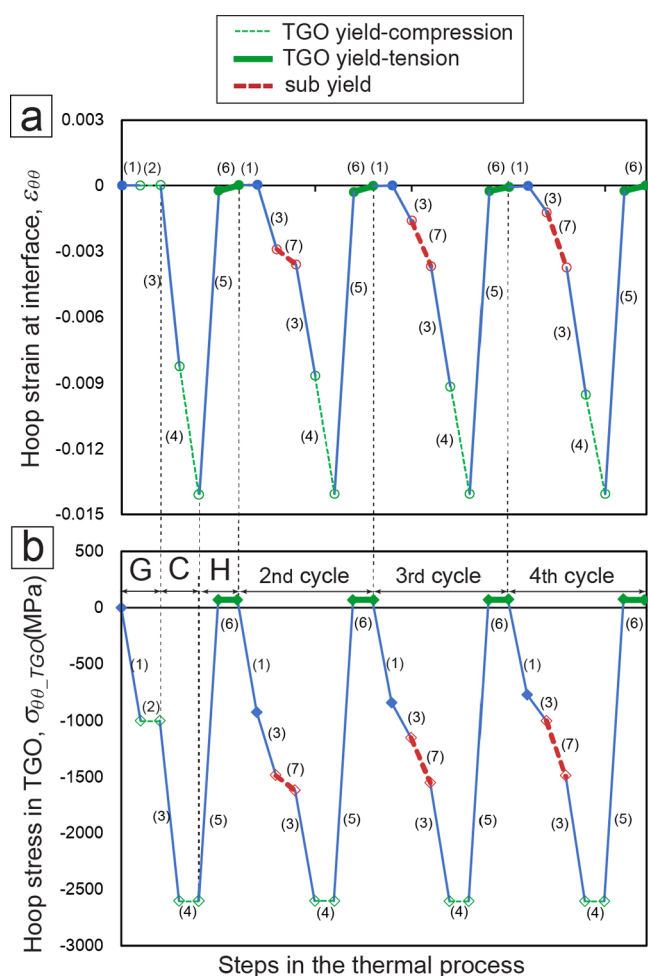
Figure 6. Analytical results of the first four thermal cycling; (a) variations of the hoop strain at the interface and (b) variation of the TGO stress (H-heating; C-cooling; G-TGO growth).

yield in this stage, and the interfacial pressure remains constant after tensile yield. The strain is given by the sum of the strains caused by the pure thermal expansion.

In the following cycles, the TGO layer does not yield again during the TGO growth.

(7) However, due to the increase of the TGO thickness, the substrate near the hole starts to yield from the second cycle. The pressure in the interface increases with the plastic region defined by R_P expansion. Eqs 15 and 16 were applied.

The yield conditions of TGO, the substrate, and TBC at each stage are shown in Table 2.

As shown in Figure 6b, the compressive stress level in TGO in which the substrate begins to yield decreases with the thermal cycles. The maximum and minimum stresses of the TGO layer are determined by the tensile strength and

compressive strength of TGO. Therefore, regardless of the number of cycles, the maximum and minimum levels are constant. On the other hand, as shown in Figure 6a, the minimum and maximum hoop strain levels at the interface nearly have no changes according to the sequence of the four cycles.

This result is quite different from the previous result of the original two-layer analytical model consisting of only the TGO layer and the substrate.[25] As shown in Figure 7, under the
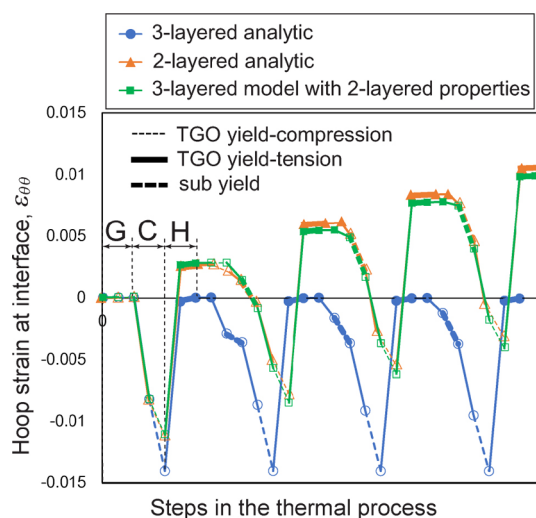

Figure 7. 3-Layer analytical results compared with 2-layer results during the first four thermal cycling.

condition that the material properties of the substrate and TGO layer are the same, the hoop strain in the two-layer model increases with the cycles elapsed. However, TBC obviously suppressed the hoop strain in the three-layer model.

In order to prove the feasibility of the 3-layer model, the following analysis proceeded. With the same condition of the material properties of TGO and the substrate, as long as TBC has no constraint on the other two layers during thermal cycling, it can be the same as the two-layer model. That is, the elastic modulus of the TBC approach is set to zero, and the CTE is set to the same value as TGO. In this way, TBC will expand or contract together with TGO and will not have a constraint on the next layer. The hoop strain comparison results with modified properties are shown in Figure 7. As shown in the figure, the hoop strain was exactly the same during the first cycle, and there was a slight difference in the stage of the TGO yield compression from the second cycle. Because according to eq 10, the thickness of TBC can only be set to tend to zero and cannot be zero. In a word, the modified three-layer model can be used to predict the deformation trend in the TBC system, and the hoop strain comparison results of the modified 3-layer model and the 2-layer model also prove the feasibility of the 3-layer model in this study.

Table 2. Yield of TGO, Substrate, and TBC at Each Stage

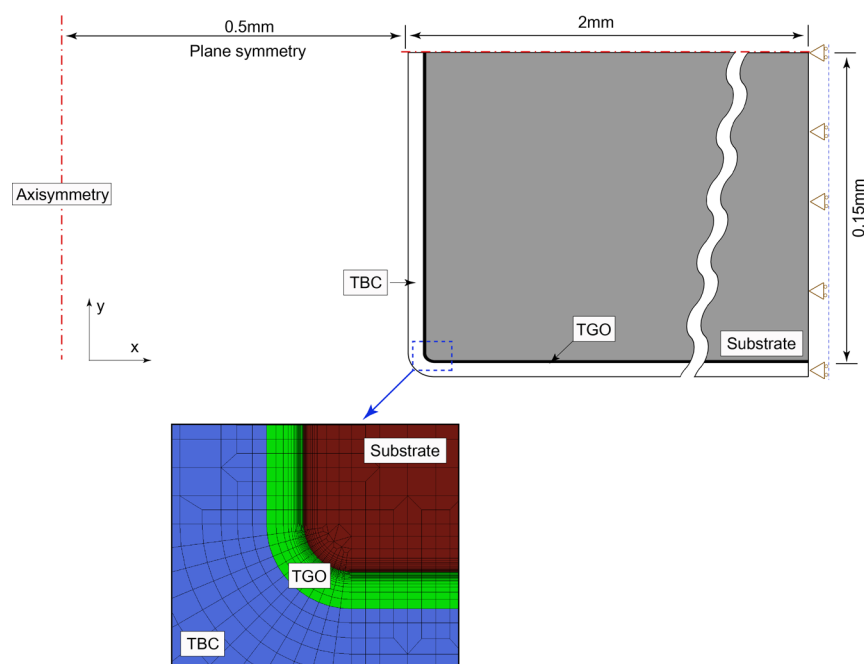| stages	1	2	3	4	5	6	7
steps	TGO growth	TGO growth	cooling	cooling	heating	heating	cooling
TGO	elastic	yield-compression	elastic	yield-compression	elastic	yield-tension.	elastic
substrate	elastic	elastic	elastic	elastic	elastic	elastic	yield
TBC	elastic	elastic	elastic	elastic	elastic	elastic	elastic

Figure 8. FEA model of the TBCs near the hole.

The first difference between the 2-layer and the 3-layer theoretical results is the yield range of TGO during cooling. As shown in Figure 7, the compressive hoop strain generated by the 2-layer model in this interval is less than that of the 3-layer model. Although tensile yield also occurs in TGO during reheating, the strain caused by tensile yield is almost very small. Therefore, under the same tensile hoop strain, the 2-layer model with small TGO compressive strain will exhibit higher strain after reheating.

The second difference between the 2-layer and 3-layer theoretical results occurred in the TGO growth stage of the second cycle. Compared to the 2-layer model, the 3-layer model did not occur in the TGO yield in the TGO growth stage of the second cycle. Since this difference occurs only once in the second cycle, it has little impact on the overall hoop strain trend.

Except for these two differences, there is no great difference between other sections. The yield of the substrate occurs only in the first half of the cooling stage, the compressive yield of TGO occurs in the second half of the cooling stage, and the tensile yield of TGO occurs at the end of the reheating stage.

5. FINITE ELEMENT ANALYSIS

In order to find out the influence of TGO and the substrate yielding based on the deformation around the cooling hole more accurately, the finite element calculation and analysis were carried out. The finite element analysis was carried out with a model which can simulate TGO and TBC on the inner and outer surfaces.

Figure 8 shows a three-layer 2D axisymmetric finite element model. The internal hole radius was set to 0.5 mm, which is the same with the analytical model. The external radius of the substrate was set to 2.5 mm because the FEA cannot make an infinite substrate; the other dimensions such as the TGO thickness and the growth rate are the same with our previous two-layer FEA model.[25] Two-layer FEA obtained almost consistent hoop strain of the cooling hole with the experimental analysis.

Compared to the 2-layer FEA model, the 3-layer model had one more TBC layer, and the thickness and growth rate of TGO exhibit no changes. The TBC thickness was set to 100 μm. Patran2011 and ABAQUS(6.10) were used for modeling and calculation.

The FEA started at the maximum temperature in a stress-free state, in which thermal history consists of cooling, reheating, and the TGO growth.

During the TGO growth, the TGO layer grows in the lateral and thickness directions. TGO growths in the lateral and thickness directions can be simulated by the ABAQUS subroutine "uexpan" and "usdfld", respectively. The details about the TGO growth simulation are described in the authors' previous work.[30,33]

The material properties were almost the same as those of the analytical solution. The difference in the behavior of TGO under compressive and tensile stress was simulated with "cast iron" provided by ABAQUS.

6. RESULTS AND DISCUSSION

Figure 9 shows the TGO hoop strain estimated by FEA for the first four thermal cycles. Compared to the analytical results shown in Figure 6, the obvious difference between the FEA and the theoretical analysis results can be seen during reheating and the subsequent TGO growth. Specifically, the substrate yields during reheating (section a in Figure 9). Because the substrate was covered by TBC and TGO on the inner and outer surfaces of the hole in the FEA model, i.e., the substrate deformation was constrained by TBC and TGO. Therefore, the substrate yields in advance at the corner around the hole (Figure 10a). After that, as the tensile yield strength of the TGO layer decreases at temperatures >900 °C, the TGO layer also yields as shown in Figure 4a (section c in Figure 9). With the further increase of the temperature, the tensile yield strength of the TGO layer decreases further, and the elasticity of the substrate is restored again (section e in Figure 9).

At the beginning of the TGO growth, the TGO growth was predetermined according to the increment of the experimental
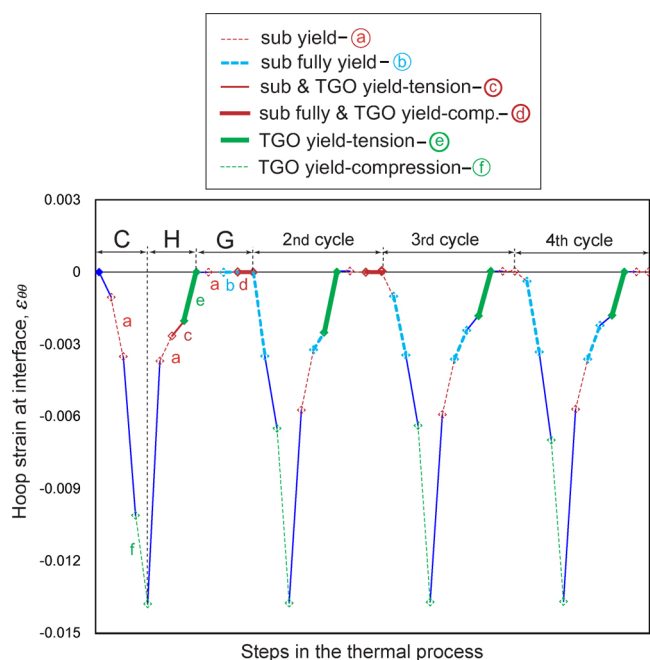
Figure 9. FEA results of the hoop strain in the TGO during the four thermal cycles. (H-heating; C-cooling; G-TGO growth).

data. With the increase of the growth strain of TGO, the substrate begins to yield again at the corner around the hole (Figure 9a) and then extends the yield area until the substrate fully yields (section b in Figure 9). Figure 10 shows the process from the beginning of the yield to full yield of the substrate during cooling and the TGO growth. The continuous growth of TGO will cause the yield of TGO itself. This phenomenon only occurs in the second and third cycles, as shown in Figure 9, which is similar with the theoretical results. The yield of TGO during the TGO growth only occurs in the first cycle in the theoretical analysis because the TGO growth rate is relatively rapid in the initial stage of the TGO growth. However, the growth is constrained by the TBC layer, which will eventually lead to the yield of TGO itself.

At the beginning of cooling, because the temperature was still high, the substrate maintains the strength at the maximum temperature, while the TGO strength increases, resulting in the substrate remaining yield and TGO returning to elasticity. Thereafter, the substrate strength increases with the decrease of the temperature, but the TGO strength remains unchanged below 900 °C; therefore, the compressive stress of the TGO layer increases until yield (section f).

Although there are some differences in details, the overall trend of hoop strain is very similar to that calculated by the analytical solution (Figure 6a). Figure 11 compares the
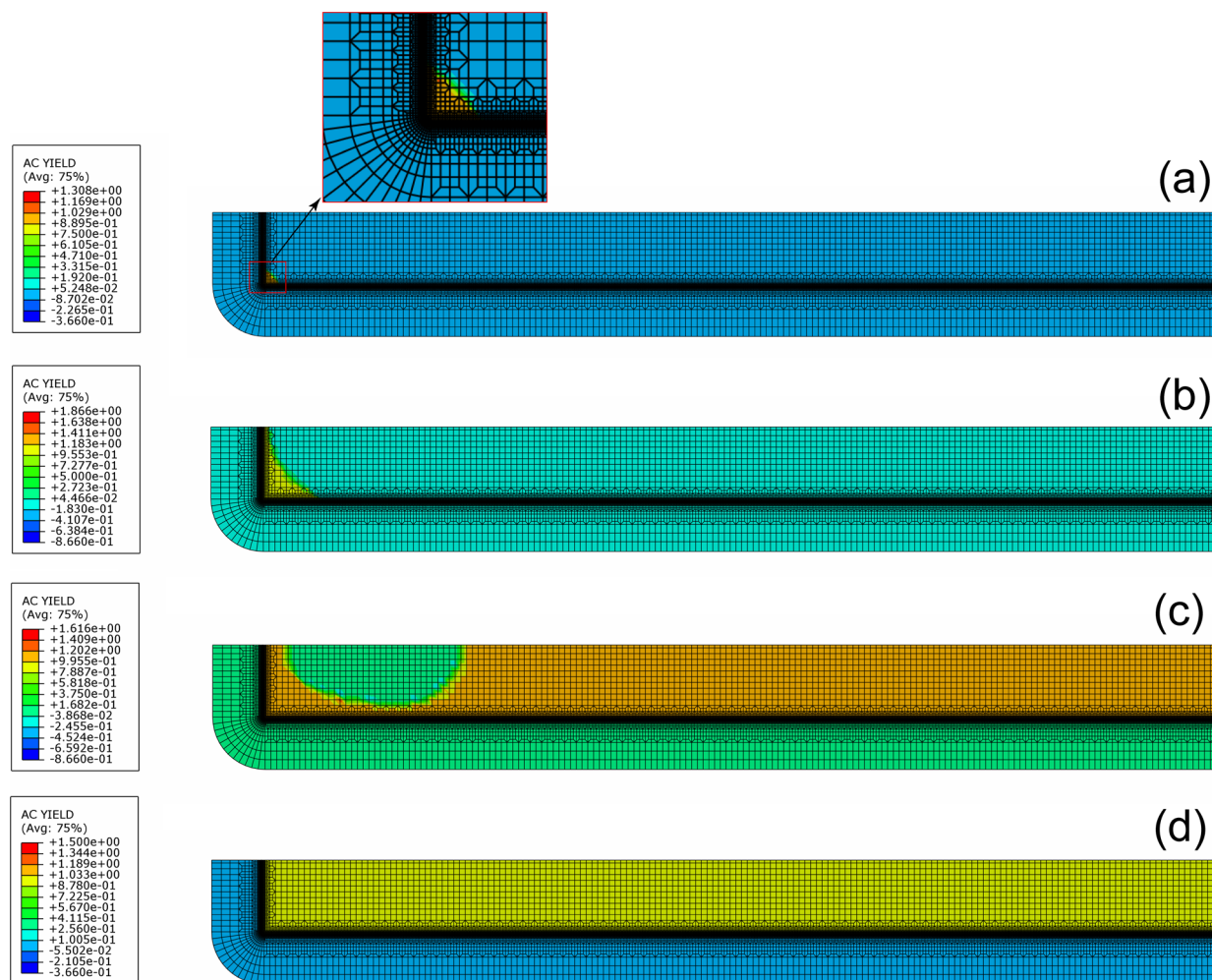

Figure 10. Substrate yield region during TGO growth and cooling; (a) substrate start to yield in the corner, (b) yield region diffuses to the center, (c) substrate almost yield, and (d) substrate fully yield.

variation of the hoop strain between the FEA and the analytical results for 10 thermal cycles. Their results are in good agreement.
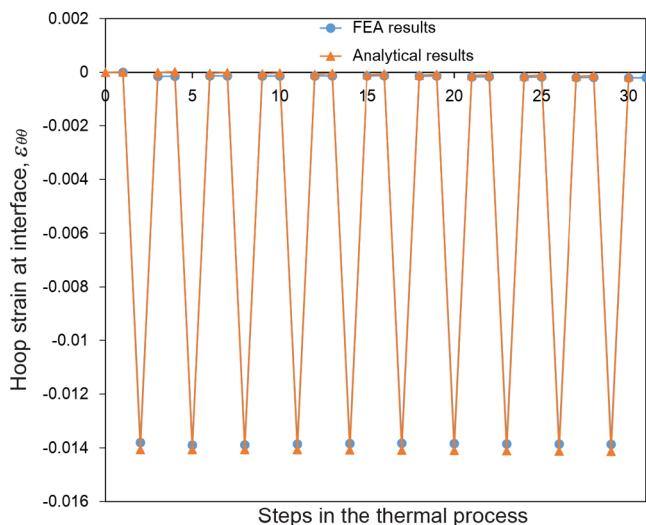

Figure 11. Comparison of the strain variation between FEA and the analytic solution.

The purpose of the FEA is to find out the reason for the strain difference around the cooling holes of the 3-layer and the original 2-layer models. The biggest difference between the strain analysis results of the two models occurs in the cooling process. Although the compression yield of TGO occurs during the cooling in both models, the hoop strain caused by TGO compression yield decreases with the increase of the cycle in the 2-layer model. However, the hoop strain produced by the 3-layer model in this interval increases gradually with the cycle. After confirming to let the TGO compression yield start temperature during cooling, it is found out that the temperature of TGO starting to yield in the first cycle is about 300 °C in both models. From the second cycle to the fourth cycle, the strain of the 2-layer model gradually decreased to about 100 °C, while the TGO compression yield starting temperature of the 3-layer model remained at about 650−600 °C.

Because the CTE of TGO is lower than the TBC layer and the substrate, TGO constrains the deformation of the substrate and TBC during cooling, which will cause thermal stress. If TGO yields, there will be no constraints to cold shrinkage and the greater strain caused by cooling. Under the same heating strain, the greater the strain produced during cooling, the smaller the residual strain that can be obtained after reheating. In other words, during cooling of the original 2-layer model, TGO resists cold shrinkage in the elastic state most of the time, and the substrate cannot shrink sufficiently. If the heating expansion strain is applied again during reheating, the strain around the cooling hole will become positive, and the strain of the cooling hole will increase with the increase of the cycle. In the developed 3-layer model, the cooling compression yield range of TGO is much larger than that of the 2-layer model, that is, during cooling, TGO has less resistance to the substrate and TBC and can produce sufficient cold shrinkage. Even if reheated, the strain value will return to a value close to the initial value. That is the main reason why the strain of the 3-layer model is much smaller than that of the 2-layer model.

As shown in Figure 11, after 10 thermal cycles, the size of the cooling hole not only does not increase but also slightly decreases. That is, the shrinkage strain during cooling is greater than the expansion strain caused by reheating and the TGO growth stage. This result also shows that TBC is very effective in the restrain deformation of TGO near the cooling hole.

In order to verify the feasibility of the 3-layer FEA model, the strain comparison data of the cooling hole in FEA, theoretical and experiment results for the 2-layer model are first shown in Table 3. As shown in Table 3, the theoretical

Table 3. Comparison of FEA, and Analytical and Experimental Results for Two-Layer and Three-Layer Models

hoop strain	two-layer	three-layer
FEA	0.00873	−6.4E−05
analytical	0.01008	−7.2E−05
experimental	0.01048	

model result was nearly the same with the experiment, and the FEA result is also close to the others. Therefore, the feasibilities of FEA and theoretical models for 2-layer problems were verified. Also, the FEA and theoretical models for 3-layer problems are listed in Table 3 which shows that there was nearly no strain of the cooling hole. Then, the strain data of original 2-layer and modified 3-layer models in every cycle were compared based on Figure 7 (Table 4). The results show

Table 4. Modified Three-Layer Analytical Results Compared with Two-Layer Results

hoop strain cycles	two-layer	modified three-layer	error
1	0.002761	0.002761	0.03%
2	0.005537	0.005409	2.31%
3	0.007901	0.007724	2.23%
4	0.010087	0.009849	2.36%

that the accuracies of the 2-layer and 3-layer models were smaller than 3%. Therefore, we can say that the theoretical and FEA models for the 3-layer problem can be verified.

7. CONCLUSIONS

This study presented the deformation resistance of TBC to the cooling holes which was analyzed by theoretical calculation and numerical simulation. The three-layer theoretical model mounted the TGO and TBC in the substrate with a cooling hole. The material strengths of the substrate and TGO, as well as the TGO growth including the lateral and thickness directions, were the experimentally measured data. Others such as the material properties of TBC were realistically assumed. Although the three-layer theoretical model only considers TBC and TGO in the inner of the cooling hole, the theoretical results are in good agreement with the numerical solution, in which the surface and inside of the cooling hole both consider the TBC and TGO layers. The detailed conclusions are as follows.

a. In the three-layer theoretical model and the numerical results, about 0.015 strain will occur during cooling and reheating, but the strain will return to the starting point after the cycle, which is very different from the results of the original two-layer model. It also shows that TBC in the three-layer

model can significantly inhibit the deformation near the cooling hole.

b. Although the three-layer model did not consider the effects of TBC and TGO on the surface of the substrate, its calculation results are consistent with the numerical results considering TBC and TGO on the surface, which proves that the three-layer theoretical model can be used to predict the deformation trend near the cooling hole during the thermal cycles.

■ AUTHOR INFORMATION

Corresponding Authors

Feng-Xun Li − *Ulsan Ship and Ocean College, Ludong University, Shandong 264025, P.R. China;* ⦿ orcid.org/0000-0002-4236-8132; Email: ldulifengxun@163.com

Zhen-Zhe Li − *College of Mechanical and Electrical Engineering, Wenzhou University, Zhejiang 325035, P.R. China;* ⦿ orcid.org/0000-0003-3356-2416; Email: a13868659593@163.com

Authors

Jian-Xin Wang − *School of Business, Ludong University, Shandong 264025, China*

Hong-Tu Sun − *Ulsan Ship and Ocean College, Ludong University, Shandong 264025, P.R. China*

Qing-Tao Gong − *Ulsan Ship and Ocean College, Ludong University, Shandong 264025, P.R. China*

Complete contact information is available at:
https://pubs.acs.org/10.1021/acsomega.3c00307

Notes

■ ACKNOWLEDGMENTS

■ NOMENCLATURE

ε_g = growth strain of the TGO layer
R_1 = outer radius of TBC
h_1 = thickness of TBC
R_2 = outer radius of TGO
h_2 = initial thickness of TGO
T_o = maximum temperature
$\Delta\varepsilon_g$ = increasing growth strain of the TGO layer
T_{RT} = room temperature
α = coefficients of thermal expansion
ΔT = temperature variation
σ_Y^{sub} = yield strength of the substrate
σ_Y^{TGO} = yield strength of the TGO layer
p_i = pressure on the inner surface
p_o = pressure on the outer surface
σ_{rr_TBC} = radial stress in the TBC layer
$\sigma_{\theta\theta\_TBC}$ = hoop stress in the TBC layer
σ_{rr_TGO} = radial stress in the TGO layer
$\sigma_{\theta\theta\_TGO}$ = hoop stress in the TGO layer

σ_{rr_sub} = radial stress in the substrate
$\sigma_{\theta\theta\_sub}$ = hoop stress in the substrate
$\varepsilon_{\theta\theta\_TBC}$ = hoop strain in the TBC layer
$\varepsilon_{\theta\theta\_tgo}$ = hoop strain in the TGO layer
$\varepsilon_{\theta\theta\_sub}$ = hoop strain in the substrate
ε_a = strain increment due to the temperature change
E = Young's modulus
G = shear modulus
ν = Poisson's ratio
R_P = radius of the plastic zone

■ REFERENCES

(1) Evans, A. G.; Mumm, D. R.; Hutchinson, J. W.; Meier, G. H.; Pettit, F. S. Mechanisms controlling the durability of thermal barrier coatings. *Prog. Mater. Sci.* **2001**, *46*, 505−553.

(2) Chellaganesh, D.; Khan, M. A.; Jappes, J. T. W. Thermal barrier coatings for high temperature applications − a short review. *Mater. Today Proc.* **2021**, *45*, 1529−1534.

(3) Hui, M.; Yu, Q.; Shi, Y. Influence of material parameters on the interfacial crack growth in thermal barrier coating system. *Ceram. Int.* **2019**, *45*, 8414−8427.

(4) Lashmi, P. G.; Ananthapadmanabhan, P. V.; Unnikrishnan, G.; Aruna, S. T. Present status and future prospects of plasma sprayed multilayered thermal barrier coating systems. *J. Eur. Ceram. Soc.* **2020**, *40*, 2731−2745.

(5) Lv, B.; Jin, X.; Cao, J.; Xu, B.; Wang, Y.; Fang, D. Advances in numerical modeling of environmental barrier coating systems for gas turbines. *J. Eur. Ceram. Soc.* **2020**, *40*, 3363−3379.

(6) Evans, A. G.; He, M. Y.; Hutchinson, J. W. Mechanics based scaling laws for the durability of thermal barrier coatings. *Prog. Mater. Sci.* **2001**, *46*, 249−271.

(7) He, M. Y.; Evans, A. G.; Hutchinson, J. W. The ratcheting of compressed thermally grown thin films on the ductile substrates. *Acta Mater.* **2000**, *48*, 2593−2601.

(8) Ranjbar-Far, M.; Absi, J.; Mariaux, G.; Dubois, F. Simulation of the effect of material properties and interface roughness on the stress distribution in thermal barrier coatings using finite element method. *Mater. Des.* **2010**, *31*, 772−781.

(9) Zhu, W.; Zhang, Z. B.; Yang, L.; Zhou, Y. C.; Wei, Y. G. Spallation of thermal barrier coatings with real thermally grown oxide morphology under thermal stress. *Mater. Des.* **2018**, *146*, 180−193.

(10) Clarke, D. R. The lateral growth strain accompanying the formation of a thermally grown oxide. *Acta Mater.* **2003**, *51*, 1393−1407.

(11) Kang, K. J.; Hutchinson, J. W.; Evans, A. G. Measurement of the strains induced upon thermal oxidation of an alumina-forming alloy. *Acta Mater.* **2003**, *51*, 1283−1291.

(12) Tolpygo, V.K.; Clarke, D.R. Wrinkling α-Alumina Films Grown by Thermal Oxidation-I. Quantitative Studies on Single Crystals of Fe-Cr-Al Alloy. *Acta Mater.* **1998**, *46*, 5153−5166.

(13) Tolpygo, V. K.; Clarke, D. R. Wrinkling α-Alumina Films Grown by Thermal Oxidation-II. Oxide Separation and Failure. *Acta Mater.* **1998**, *46*, 5167−5177.

(14) Krewinkel, R. A review of gas turbine effusion cooling studies. *Int. J. Heat Mass Transfer* **2013**, *66*, 706−722.

(15) Song, M.; Ma, Y.; Gong, S. K. Analysis of residual stress distribution along interface asperity of thermal barrier coating system on macro curved surface. *Prog. Nat. Sci.: Mater. Int.* **2011**, *21*, 262−267.

(16) Kumar, V.; Balasubramanian, K. Progress Update on Failure Mechanisms of Advanced Thermal Barrier Coatings. *Prog. Org. Coat.* **2016**, *90*, 54−82.

(17) Bogard, D. G.; Thole, K. A. Gas turbine film cooling. *J. Propul. Power* **2012**, *22*, 249−270.

(18) Tu, Z.; Li, C.; An, B.; Liu, J.; Xu, G. Experimental investigation of film cooling effectiveness on a gas turbine blade pressure surface with diffusion slot holes. *Appl. Therm. Eng.* **2019**, *168*, No. 114851.

(19) Li, Z.; Gao, H.; Wen, Z.; Yang, Y.; Yue, Z. Microcrack initiation behavior around film cooling holes in a Ni-based single crystal: in situ observation and crystal plastic analysis. *Mater. Sci. Eng., A* **2020**, *771*, No. 138609.

(20) Zhao, T.; Hu, X.; Jing, Y.; Teng, X.; Liu, F.; Li, B.; Zhang, S.; Sun, Y. Creep-fatigue rupture mechanism and microstructure evolution around film-cooling holes in nickel-based DS superalloy specimen. *Intermetallics* **2021**, *169*, No. 107359.

(21) Jiang, J.; Wu, D.; Wang, W.; Zhao, X.; Ma, X.; Wang, B.; Shi, H. J. Fracture behavior of TBCs with cooling hole structure under cyclic thermal loadings. *Ceram. Int.* **2020**, *46*, 3644−3654.

(22) Rebollo, N. R.; He, M. Y.; Levi, C. G.; Evans, A. G. Mechanisms governing the distortion of alumina-forming alloys upon cyclic oxidation. *Z. Metallkd.* **2003**, *94*, 171−179.

(23) Karlsson, A. M.; Hutchinson, J. W.; Evans, A. G. The displacement of the thermally grown oxide in thermal barrier systems upon temperature cycling. *Mater. Sci. Eng., A* **2003**, *351*, 244−257.

(24) Karlsson, A. M.; Hutchinson, J. W.; Evans, A. G. A fundamental model of cyclic instabilities in thermal barrier systems. *J. Mech. Phys. Solids* **2002**, *50*, 1565−1589.

(25) Li, F. X.; Kang, K. J. Deformation and cracking near a hole in an oxide forming alloy foil subjected thermal cycling. *Acta Mater.* **2013**, *61*, 385−398.

(26) Li, F.-X.; Kang, K.-J. Deformation and cracking near a hole in an oxide forming alloy foil subjected to thermal cycling. Part II: Effects of remotely applied stress. *Acta Mater.* **2013**, *61*, 2944−2952.

(27) Li, F. X.; Li, Z. Z. Multi-objective global optimization for deformation near a hole in an oxide forming alloy foil subjected to thermal cycling. *Int. J. Precis. Eng. Manuf. − Green Technol.* **2018**, *5*, 261−269.

(28) Saada, A.S. *Elasticity theory and applications*; Pergamon Press Inc.: New York, 1974; pp 323−329.

(29) Kaliszky, S. *Plasticity: theory and engineering applications*; Elsevier: New York, 1989; pp 168−175.

(30) Ding, J.; Li, F.-X.; Kang, K.-J. Effects of material creep on displacement instability in a surface groove under thermo-mechanical cycling. *Surf. Coat. Technol.* **2009**, *204*, 157−164.

(31) Sharma, S. K.; Ko, G. D.; Kang, K. J. High temperature creep and tensile properties of alumina formed on FeCr alloy foils doped with yttrium. *J. Eur. Ceram. Soc.* **2009**, *29*, 355−362.

(32) Kang, K. J.; Mercer, C. Creep Properties of a Thermally-Grown Alumina. *Mater. Sci. Eng., A* **2008**, *478*, 154−162.

(33) Ding, J.; Li, F.-X.; Kang, K.-J. Numerical simulation of displacement instabilities of surface grooves on an alumina forming alloy during thermal cycling oxidation. *J. Mech. Sci. Technol.* **2009**, *23*, 2308−2319.